JOURNAL OF AIRCRAFT
Vol. 39, No. 1, January–February 2002

Tail Buffet Alleviation Through the Use of Wing–Strake Fillet Shapes

Terence A. Ghee,* Hugo A. Gonzalez,† and David B. Findlay‡
U.S. Naval Air Systems Command, Patuxent River, Maryland 20670-1906

Various fillet shapes at the strake–wing juncture of a 76/40 deg double-delta wing model were experimentally investigated to gauge the effect of the fillet in alleviating adverse vortex/tail interaction. The vertical tails were instrumented with 28 fast-response pressure transducers. Pressure time histories and frequency power spectral densities were analyzed for four wing–strake fillet configurations and at three spanwise tail locations. Angle of attack was varied from − 2 to 40 deg, tunnel dynamic pressure was 26.74 psf (1280 pascals), and Reynolds number was 1.3×10^6. The results show that the fillet geometry can increase or decrease tail buffet in comparison to the baseline, no fillet case. Linear and parabolic fillet shapes were found to increase tail buffet above the baseline case. A diamond fillet shape was found to alleviate tail buffet and shift the tail buffet to a higher frequency. The use of such a shape on flight vehicles may result in a longer fatigue life of the vertical tails.

Nomenclature

A	=	constant, b/V_∞, 0.0091/s
AR	=	aspect ratio, 2.41
a_∞	=	speed of sound, 1155 ft/s, 352 m/s
b	=	span, 1.36 ft, 0.414 m
C	=	coherence
C_P	=	pressure coefficient, $p - p_\infty/q_\infty$
c	=	chord, ft, m
c_R	=	root chord, 1.33 ft, 0.405 m
$c_{R\text{tail}}$	=	tail root chord, 0.38 ft, 0.116 m
c_t	=	tip chord, 0.21 ft, 0.064 m
$c_{t\text{tail}}$	=	tail tip chord, 0.13 ft, 0.040 m
f	=	frequency, Hz
G	=	amplifier gain
I_{raw}	=	raw integer value (digital)
M_∞	=	freestream Mach number, V_∞/a_∞, 0.13
P	=	pressure, psf
P_{ref}	=	reference pressure, psf
q_∞	=	tunnel dynamic pressure, 26.74 psf, 1280 pascals
Re	=	Reynolds number, $(\rho_\infty V_\infty C_R)/\mu_\infty$, $1.3E6$
S	=	wing area, 0.768 ft^2, 0.071 m^2
Se	=	transducer sensitivity, V/psf
Sr	=	Strouhal number, $(bf)/V_\infty$
S_{tail}	=	tail area, 0.093 ft^2, 0.009 m^2
t	=	time, s
$t_{\max}$	=	model maximum thickness, 0.0313 ft, 0.001 m
V	=	excitation voltage, 10 V
V_∞	=	tunnel freestream velocity, 150 ft/s, 46.7 m/s
α	=	geometric angle of attack, deg
λ	=	taper ratio, 0.16
λ_{tail}	=	tail taper ratio, 0.33
μ_∞	=	viscosity, $3.7373E-7$, slug/(ft · s), $1.7894E-5$ kg/(m · s)
τ	=	nondimensional time, $(ta_\infty)/cR$

Received 5 August 2000; revision received 1 November 2000; accepted for publication 15 July 2001.

*Aerodynamicist, NAVAIR 4321, Building 2187, Suite 1320B. Senior Member AIAA.
†Aerodynamicist, NAVAIR 4322, Building 2187, Suite 1320B. Senior Member AIAA.
‡Advanced Aerodynamics Branch Head, NAVAIR 4321, Building 2187, Suite 1320B. Member AIAA.

Introduction

MODERN fighter/attack air vehicles rely on vortex lift to allow the vehicle to achieve high-angle-of-attack flight. Typically, a leading-edge extension (LEX) is combined with a modified delta wing. The LEX surface creates a pair of vortices that generate significant lift. However, the use of vortex lift is not without a downside. Impingement of the burst LEX vortices on the vertical tail of a modern fighter/attack air vehicle was found to cause fatigue and premature replacement of the vertical tails. It is thought that the breakdown of the LEX vortex impinged on the vertical tails at a frequency close to a structural vibratory mode. Many researchers in recent years have focused on quantifying the effect of the LEX vortex on vertical tails.[1–5]

Wing–strake fillets on double-delta wings have been investigated by various U.S. Navy researchers to determine fillet effect on forces and moments and flowfield structure.[6–11] As part of a continuing effort into the effects of fillet shapes on vertical tail buffet, a wind-tunnel test was conducted using a 76/40 deg double-delta wing with instrumented vertical tails. In addition, the vertical tails were moved spanwise. Pressure time histories were recorded and analyzed in the time and frequency domains to quantify the response sensed on the vertical tails to the vortex forcing.

Experimental Apparatus

The tests were conducted in the U.S. Naval Aerodynamic Test Facility (NATF). The NATF is a 4 ft × 4 ft (1.2 m × 1.2 m) closed test section, open-return wind tunnel. The facility incorporates a 200-hp motor that drives a variable pitch fan and delivers a maximum velocity of 205 ft/s (62.5 m/s). In addition, the facility has honeycomb and three sets of flow conditioning screens. Figure 1 shows the 76/40 deg double-delta wing in the NATF.

The model used in the present investigation consisted of a 76/40 deg double-delta wing with vertical tails mounted on booms aft of the wing. Manufactured of stainless steel, the model featured a flat upper surface with sharp, 20-deg beveled edges (see Fig. 2).

Four sets of fillets (shown in Fig. 3) were used in the present investigation: a baseline (no fillet, F1), linear (F2), diamond (F3), and parabolic (F4). Each fillet planform area was 1% of total wing planform area. Thus, starboard and port fillets combined to total 2% of the wing planform area. Details of the fillet geometry, design, and effect on aerodynamic performance may be found in Refs. 6 and 7.

The rigid vertical tails were attached to booms that were then mounted to the underside of the wing. The booms were positioned at three spanwise locations (see Fig. 4). The tails were instrumented with 28 Kulite® fast-response, differential-gauge pressure

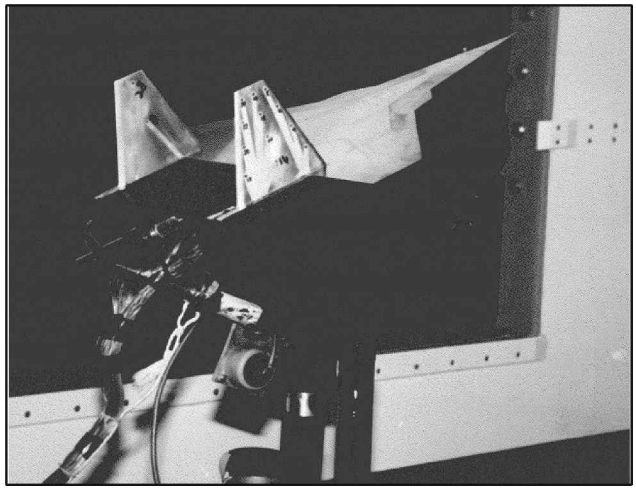

Fig. 1 Double-delta 76/40 deg wing in NATF.

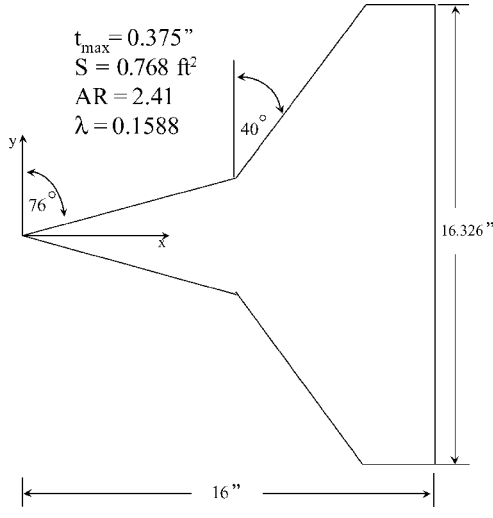

Fig. 2 Schematic of 76/40 deg double-delta wing.

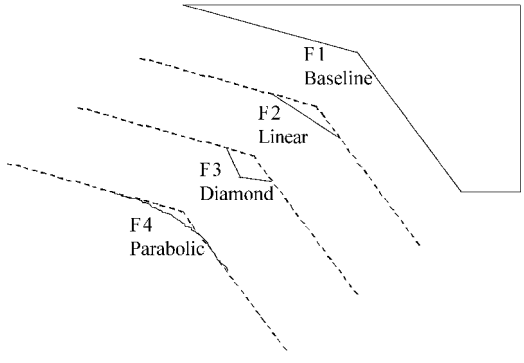

Fig. 3 Fillet geometry.

transducers: The starboard tail had 12 transducers on the inboard and outboard side (see Fig. 5). The port tail had transducers located equivalent to transducers 9, 10, 13, and 14 on the starboard tail. These port tail transducer locations proved unfortunate as the strongest response was seen along the leading edge of the vertical tails. The tails were positioned normal to the wing surface and had an 18.43-deg leading- and trailing-edge sweep angle. A cover plate spanned the area between the tails and mitigated the effect of the flow on the under surface from the flow on the upper surface.

A short sting assembly attached to the facility pitch strut supported the model. Because of an error in mounting the support system turntable, a −1.344-deg sideslip angle was introduced. In

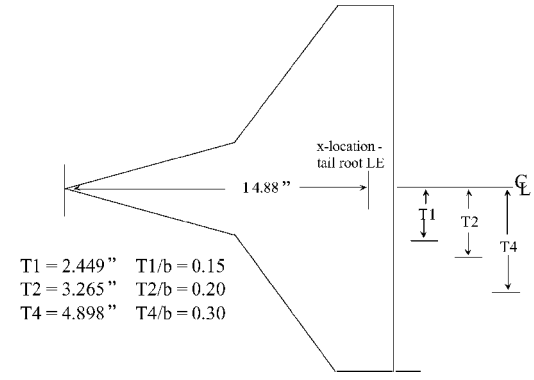

Fig. 4 Vertical tail location.

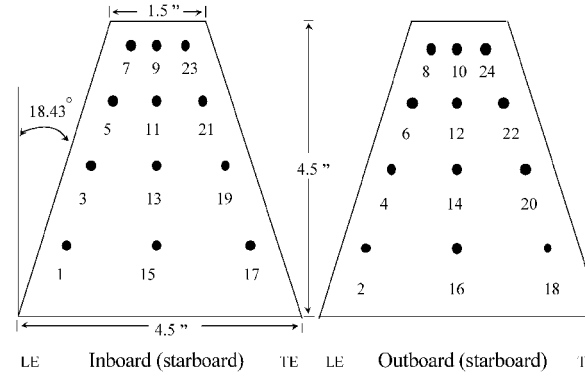

Fig. 5 Transducer location on vertical tails.

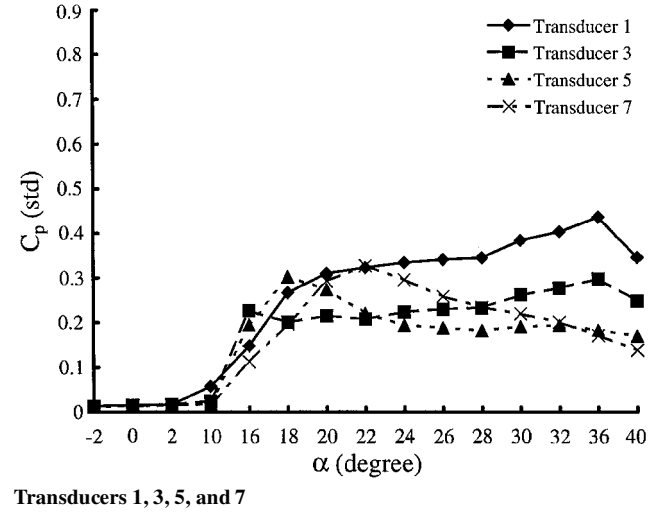

Transducers 1, 3, 5, and 7

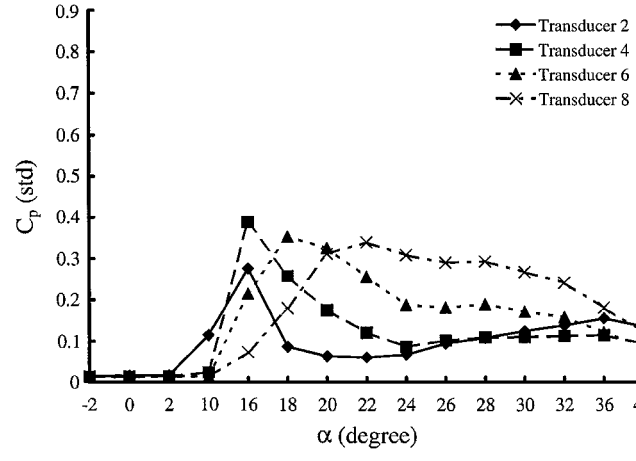

Transducers 2, 4, 6, and 8

Fig. 6 C_p (standard deviation) vs α, F1T2.

recent tests in the NATF, the crossflow angle was determined to be −0.09 deg. Thus, the error in sideslip was −1.254 deg. Also, the support system was constrained vertically; the model moved off centerline with changing angle of attack. However, velocity surveys of the tunnel test section have shown the difference in flow uniformity to be less than 1%.

The data were acquired using a Sheldon SI-100 16-bit, 32-input data-acquisition system connected to a personal computer. This system sampled the data in a multiplex fashion. Thus, data coincidence was not possible with this system. However, the time shift between data taken at a subsequent channel was 2.0 μs. The worst case would be the difference in time between channel 1 and 32 and corresponded to 64 μs, but was still almost double the data sampling rate.

Procedure and Data Reduction

The tests were conducted at a constant tunnel velocity of 150 ft/s (45.7 m/s) [$q_\infty = 26.74$ psf (1280 pascals) and Reynolds number of 1.3×10^6 based on root chord]. Model incidence was varied from −2 to 40 deg, more specifically, −2, 0, 2, 10, 16, 18, 20, 22, 24, 26, 28, 30, 32, 36, and 40 deg. Before tunnel startup, 5 s of wind-off-zero data were acquired. The transducers were then nulled, and the tunnel was driven to 150 ft/s. After test conditions steadied, unsteady pressure data were acquired. Unsteady tail pressures were sampled at 8192 samples/s for 30 s. A Bessel filter provided a low-pass cutoff frequency of 2212 Hz. Following tunnel shutdown, wind-off-zero data were acquired for comparison to the pretest wind-off-zero data. The tails were tested at the most forward location on the booms at three spanwise locations (T1, T2, and T4 in Fig. 4) for each fillet and the baseline configuration.

The data were first analyzed to cull the vast amount of data to a workable amount. A custom Labview software routine was used to look at all of the data and choose those configurations where significant tail/vortex interactions occurred. In this manner, approximately 120 configurations were perused and reduced to 35 configurations to be analyzed. For each of the 35 configurations, all 28 transducers were evaluated to determine the time history and power spectral density (PSD) characteristics.

The large size of the data array (245,760 samples per transducer per run) necessitated the data be analyzed on a high-performance computer system. MATLAB® software was used to determine the pressure time history and pressure PSD using an SGI Power Challenge Array located at the U.S. Army Research Laboratory (ARL).

The data were converted to engineering units using the following:

$$P - P_{\text{ref}} = \frac{[(I_{\text{raw}} \times V)/65{,}535]}{G \times Se} \tag{1}$$

in pounds per square foot. The assumption was made that the wind-off-zero pressure was total pressure. At the time of the test, a barometric pressure device was not available. Thus, tunnel static pressure was determined by subtracting the tunnel dynamic pressure from the wind-off-zero (or total) pressure. Pressure coefficient data were determined by the following:

$$C = \{[(P_{\text{measured}} - P_{\text{ref}}) - (P_{\text{wind-off zero}} - P_{\text{ref}})] - q_\infty\}/q_\infty \tag{2}$$

The coherent acoustic noise present in the freestream data was removed from the tail pressure measurements by assuming the model oriented at 0-deg incidence measured freestream noise. Although the use of zero-angle-of-attack data to remove the acoustic noise content is not true coherence, an unsteady static pressure probe

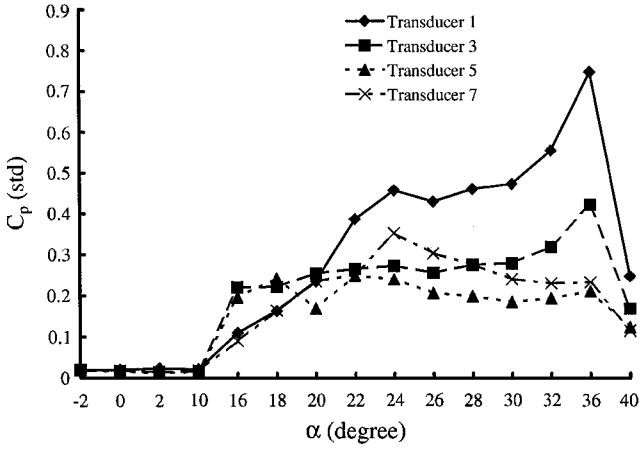

Transducers 1, 3, 5, and 7

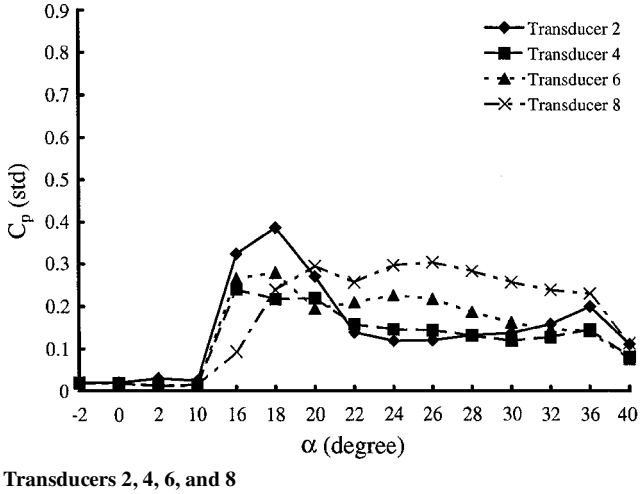

Transducers 2, 4, 6, and 8

Fig. 7 C_p (standard deviation) vs α, F2T2.

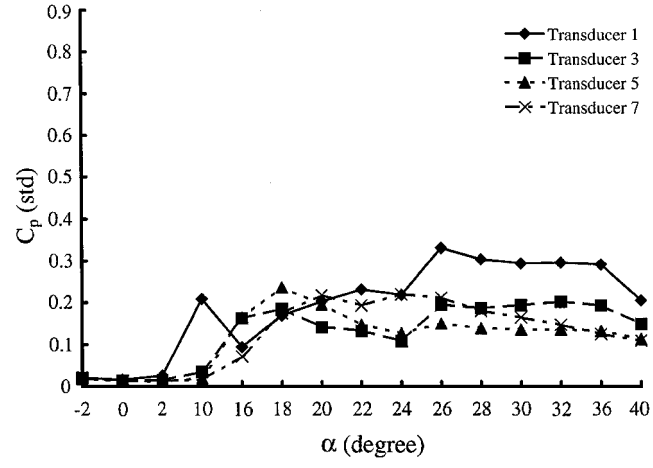

Transducers 1, 3, 5, and 7

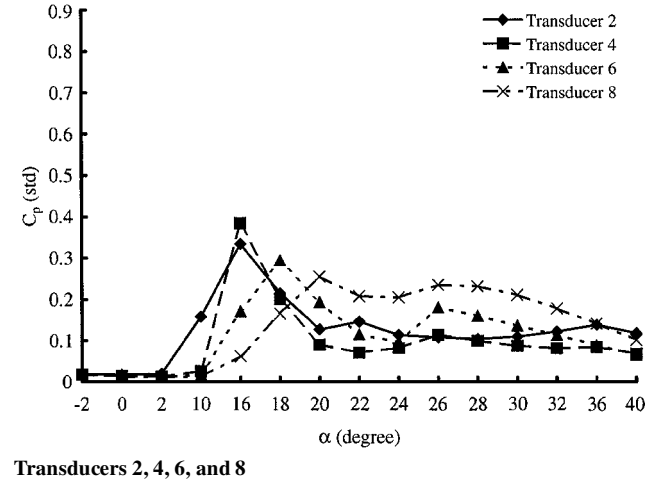

Transducers 2, 4, 6, and 8

Fig. 8 C_p (standard deviation) vs α, F3T2.

was unavailable for the present study. However, use of zero-angle-of-attack data at least allowed the removal of the wind-tunnel fan contamination. The coherence was a function of the power spectrum of the freestream noise (determined when the model was at zero incidence) and the power spectrum of the data at an arbitrary angle of attack and the cross spectrum of the freestream noise and the data at the arbitrary angle of attack (see Refs. 1 and 12). Thus, the coherence was found by

$$C = \frac{(\mathrm{PSD}_{\mathrm{zero,meas}})^2}{(\mathrm{PSD}_{\mathrm{zero,zero}}) \times (\mathrm{PSD}_{\mathrm{meas,meas}})} \tag{3}$$

The PSD of the measured data is then

$$\mathrm{PSD}_{\mathrm{meas}} = (1 - C) \times \mathrm{PSD}_{\mathrm{meas,uncorrected}} \tag{4}$$

(rms^2).

The algorithm to determine the PSD was based on the method by Welch.[13] The data were segmented into windows to allow 30 averages and corresponded to a frequency resolution of 1 Hz. No data overlapping was employed, and a Hanning filter was used with a window length the same size as the data segments. The mean was eliminated from the PSD and coherence calculations, and a 95% confidence criterion was used to gauge the PSD assessment.

The surface pressure excitation spectra are presented as a nondimensional rms pressure fluctuation as recommended for buffet tests by Mabey[14]:

$$(Sr \times \mathrm{PSD})^{0.5} \qquad \text{or} \qquad (A \times f \times \mathrm{PSD})^{0.5} \tag{5}$$

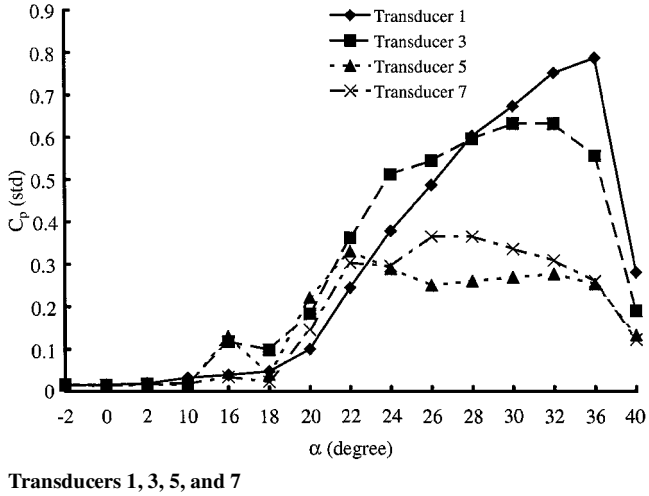

Transducers 1, 3, 5, and 7

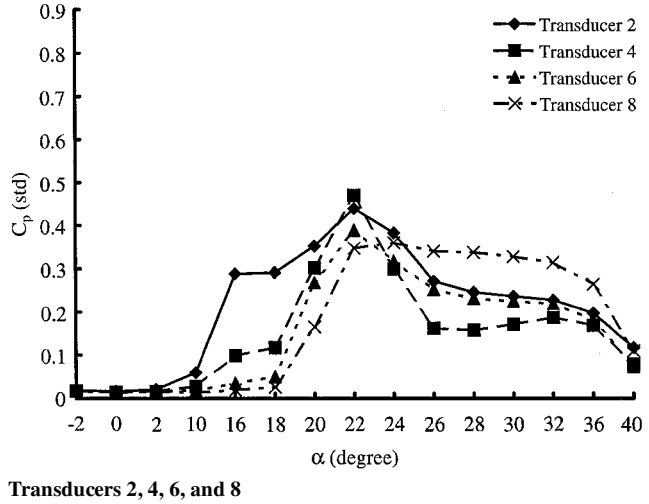

Transducers 2, 4, 6, and 8

Fig. 9 C_p (standard deviation) vs α, F4T2.

Thus, the amplitude of the PSD is weighted by multiplying the incremental frequency to the corresponding PSD amplitude. This method reduced PSD amplitudes occurring at low frequencies.

An uncertainty estimate of the data was undertaken to gauge the accuracy of the test results. The unsteady pressure measurement accuracy was driven by the quoted instrumentation repeatability of 0.1%. The effect of the accuracy of the A/D system and power supply was evaluated and found to have limited impact on the data accuracy (the effect, however, was incorporated in the error analysis). As noted earlier, the tunnel velocity varied in the test section by approximately 1% and fluctuated by approximately 0.75% at the tested tunnel velocity. When a method outlined by Rae and Pope[15] was used, the uncertainty in pressure coefficient was estimated to be 0.027. The highest and lowest resolvable frequencies were 2212 and

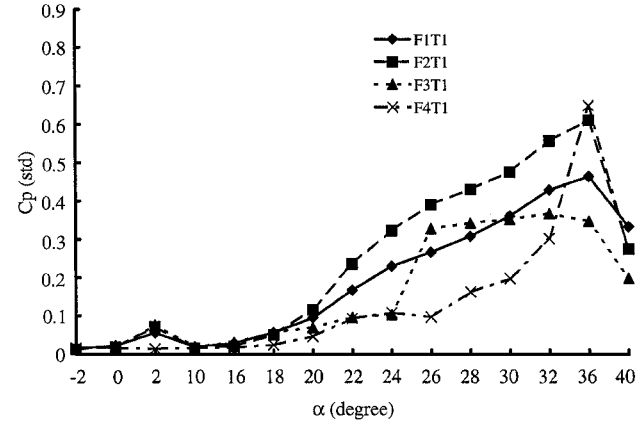

a) Tail position 1

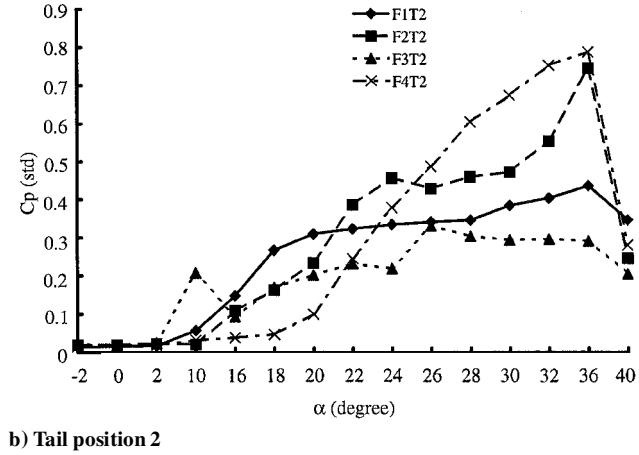

b) Tail position 2

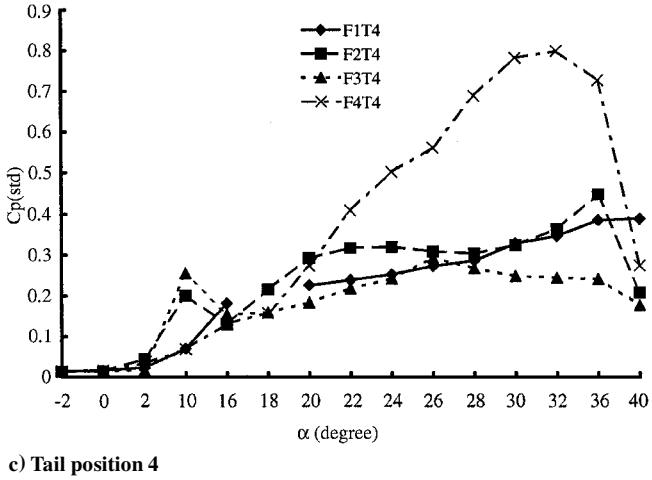

c) Tail position 4

Fig. 10 C_p (standard deviation) vs α, transducer 1.

0.03 Hz, respectively, based on the sample rate, filters employed, and dwell time. However, the frequency resolution of the PSD, as quoted earlier was 1 Hz.

Results

Buffet Standard Deviation

The pressure time histories were analyzed to determine the standard deviation from the mean as a gauge of the relative strength of the tail buffet. Note, the notation F number T number is used to describe the fillet shape and tail position. For example, F1T2, is the baseline fillet with the tails in position 2 (see Figs. 3 and 4 for the other fillet and tail notations).

As shown in Figs. 6–9, tail pressure buffet response standard deviation, in coefficient form, is plotted vs angle of attack for transducers along the leading edge of the starboard tail. Maximum standard deviation from the mean pressure generally occurred at the inboard root leading edge. In fact, quite often the pressures calculated

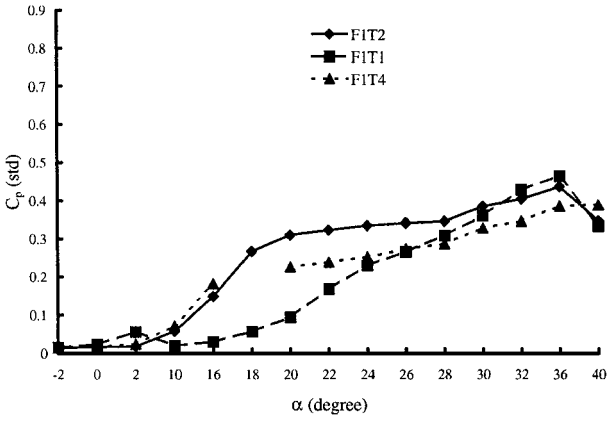

Baseline fillet

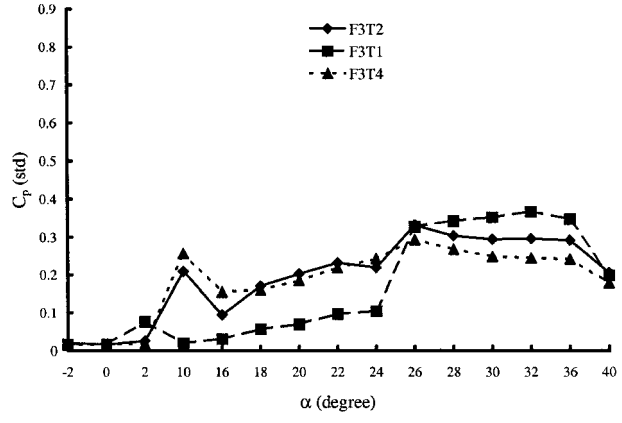

Diamond fillet

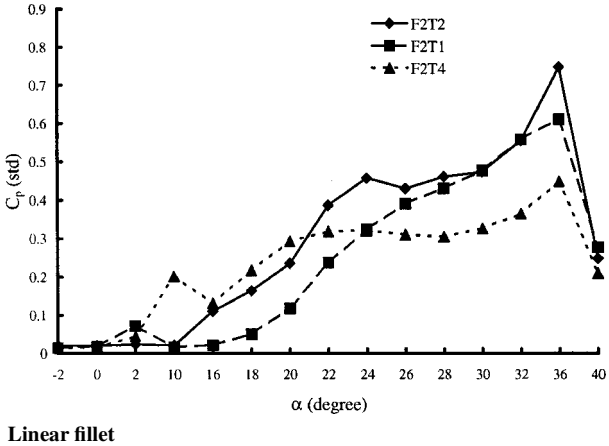

Linear fillet

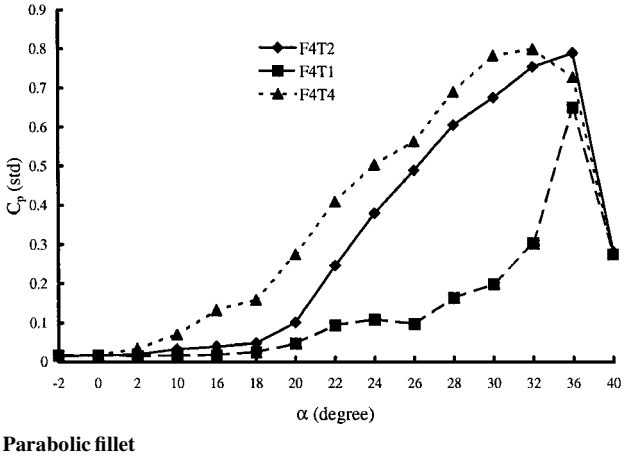

Parabolic fillet

Fig. 11 C_p (standard deviation) vs α, transducer 1.

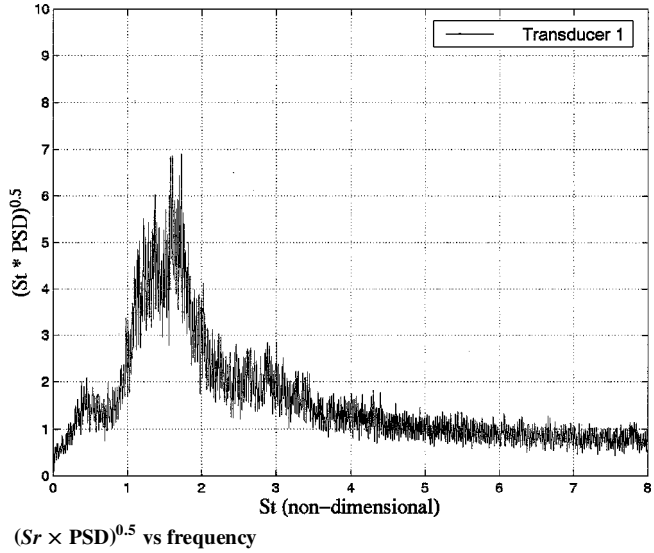

$(Sr \times \text{PSD})^{0.5}$ vs frequency

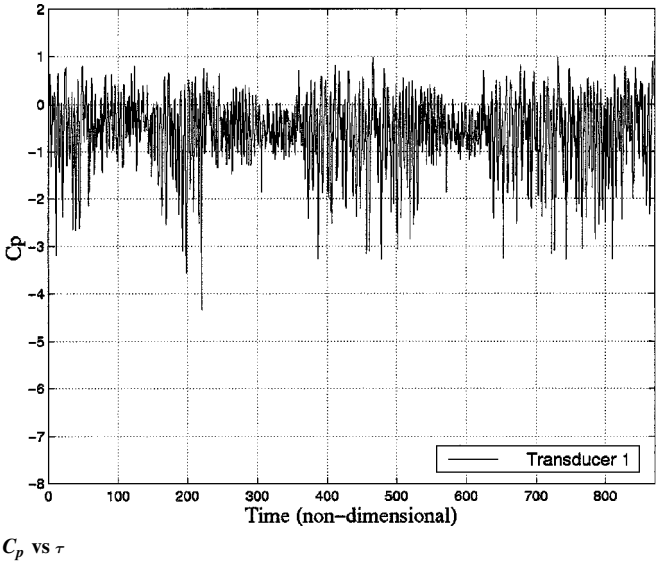

C_p vs τ

Fig. 12 Transducer 1 (inboard), $\alpha = 32$ deg, F4T2.

for the other transducer locations were quite insignificant by comparison. Therefore, the port tail transducers, which were located along the tail centerline proved to sense rather low levels of tail buffet.

In general, maximum buffet pressure response occurred on the inboard side of the tail leading edge for the various fillet shapes tested. The outboard leading-edge pressure transducer locations were seen to have buffet peaks at angles of attack significantly lower than the inboard leading-edge pressure transducer locations (16–22 deg for the outboard locations as opposed to 32–36 deg for the inboard transducers, c.f., Fig. 9). The mean pressure was analyzed on the tails and was noted to vary little with transducer location.

Figure 10 is a comparison of the effect of fillet shapes on tail buffet pressure response at the inboard root leading edge (transducer 1) for different tail positions. The parabolic fillet was seen to generate the maximum tail buffet, followed by the linear fillet. The diamond fillet was seen to generate the least amount of tail buffet. In addition to the reduced tail buffet pressure signature of the diamond fillet, in Ref. 6, the use of diamond fillets (as well as the other fillets) is reported to increase significantly the maximum lift coefficient by 18%. The diamond fillet may also have the advantage of reduced low observable (LO) characteristics. However, these results must be viewed with caution, because the configuration did not utilize a fuselage. A recent report has shown the effect of fillets on a representative modern fighter/attack vehicle to have little effect on the aerodynamic lift.[11]

As seen in Fig. 10c, the parabolic fillet exhibited substantially more tail buffet for the tails positioned farthest outboard. It is due to the manner that the vortex is formed that explains this difference. In Refs. 6 and 7 computational fluid dynamics (CFD) streamlines of the flow over the wing are presented. It was found that the strake vortex smoothly combined with the wing vortex into essentially one large vortex system. This parabolic fillet vortex system appeared to be more outboard of the vortices generated by the other fillets. Also, because there were no wing–strake leading-edge discontinuities, the vortex system was stronger. The diamond fillet, by comparison, creates a number of vortices from each leading-edge discontinuity (see Refs. 6–8). Thus, it is not surprising that the parabolic fillet provides the strongest tail buffet pressure response and the diamond fillet provides the weakest tail buffet pressure response. Note that similar trends of the effect on fillet shape on tail buffet were seen at other transducer locations.

The effect of tail position on buffet pressure response, for a given fillet, failed to provide a consistent pattern, as seen in Fig. 11. In general, for a given fillet, the curves exhibited the same general shape.

Table 1 Maximum amplitude with corresponding frequency

Sr	Amplitude $(Sr \times \text{PSD})^{0.5}$	Transducer	α
	F1T2		
1.1244	2.5731	1	30
1.0876	2.9825	1	32
1.0876	3.3041	1	36
	F2T2		
1.6590	4.9708	1	32
1.5115	7.0468	1	36
	F3T2		
1.8433	3.2164	4	16
1.7512	2.1345	1	30
1.7512	2.2807	1	32
	F4T2		
1.8986	7.3392	4	22
1.7143	9.1452(C)	3	30
1.7143	6.9006	1	32
	F1T1		
1.5115	5.1170	6	22
1.4009	2.3099	1	30
1.3088	2.8363	3	32
1.2719	3.3918	3	36
	F2T1		
2.3410	1.9006	3	22
2.5806	2.8070	3	24
1.5668	4.4444	1	32
1.3641	4.6199	3	36
	F3T1		
1.6037	2.1637	3	30
1.6221	3.3041	1	32
	F4T1		
1.4931	7.0468	6	30
1.3273	7.1930	8	32
	F1T4		
1.6221	2.4561	7	24
1.1244	2.3977	1	32
1.0691	2.2515	1	36
1.2166	3.0944	1	40
	F2T4		
1.4009	2.4854	1	32
1.3641	3.7427	1	36
	F3T4		
1.5115	1.8713	8	20
1,6959	1.6959	1	32
1.4931	1.3743	1	36
	F4T4		
1.7880	8.5673(C)	1	26
1.2535	7.6023(C)	1	32
1.2535	7.1053	1	36

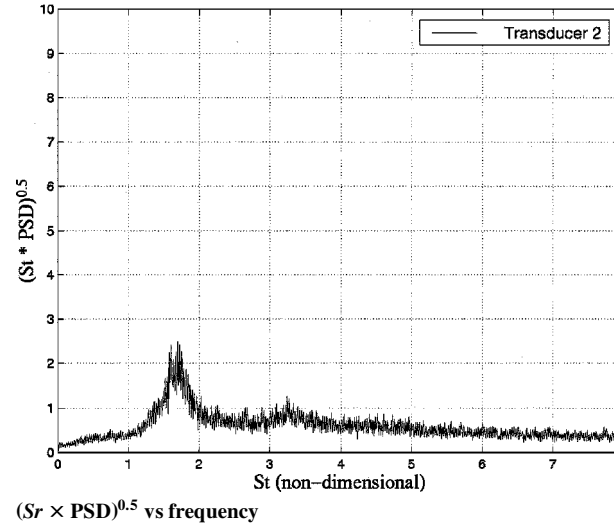

$(Sr \times \text{PSD})^{0.5}$ vs frequency

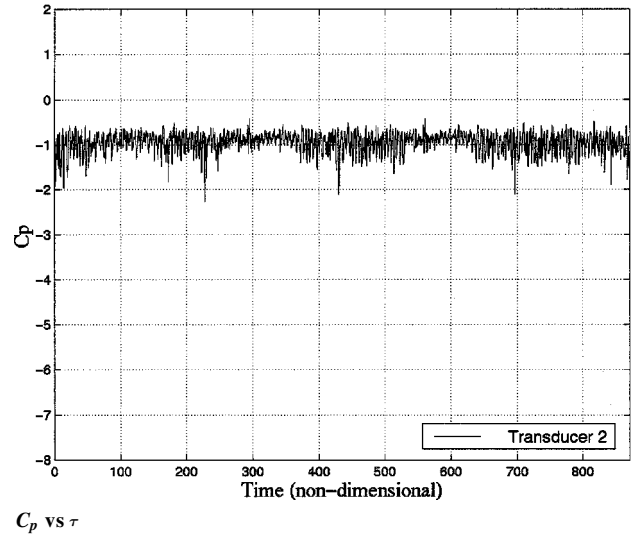

C_p vs τ

Fig. 13 Transducer 2 (outboard), $\alpha = 32$ deg, F4T2.

PSD and Time History Plots

Table 1 is a summary of the location of the maximum weighted PSD amplitude, $(Sr \times \mathrm{PSD})^{0.5}$, and corresponding frequency for a given configuration. That is, for a given configuration (angle of attack, fillet shape, etc.) all transducers were analyzed to find a single maximum weighted value for PSD amplitude and corresponding frequency. Amplitude data annotated with a C in Table 1 indicate that the data were clipped (the signal was overdriven).

Analysis of the location of the maximum peak of weighted PSD amplitude frequencies showed the peak to occur along the leading edge of the vertical tails. A majority of the frequencies were shown to occur at the inboard root leading edge (transducer 1). Furthermore, analysis showed that the frequency of the maximum amplitude varied with fillet shape, tail location, transducer location, and angle of attack. Significant amplitude values existed on the tail at frequencies different than those reported in Table 1. For example, it was noted that the frequencies along the tail tip were often different from the frequency measured along the root leading edge. The frequency also varied inboard vs outboard. Therefore, quantifying the frequency of the buffet pressure response does not easily lend itself to a single value.

Figures 12 and 13 show the difference in a buffet response inboard vs outboard at the root leading edge for a parabolic fillet for tail location 2 at 32-deg angle of attack. The inboard transducer recorded a higher buffet value, perhaps as a result of the rotation of the vortex system. It may also be influenced by vortices associated with the vertical tail itself. In Fig. 12, the peak frequencies correspond well inboard vs outboard. However, this trend was not always followed.

As noted earlier, the parabolic fillet was seen to produce the greatest amount of tail buffet, and the diamond was seen to experience the least amount of tail buffet. This trend is borne out in Fig. 14 by viewing the peak weighted PSD amplitude for each configuration. The data presented in Fig. 14 are located on the starboard tail, inboard root leading edge (transducer 1) for an angle of attack of 32 deg and tail position 2 and are representative of the frequency-domain database. In addition to the diminished amplitude of the diamond fillet configuration, the characteristic frequency was seen to be higher than the baseline configuration characteristic frequency. Such a frequency increase could be beneficial by shifting the characteristic frequency of the vortex system away from the natural frequency of the tails. Thus, buffet alleviation can occur by reducing the amplitude or moving the characteristic frequency of the vortex system away from the tail natural frequency.

The corresponding nondimensional time history plots for this configuration are presented in Fig. 15 and represents 1 s of data. The diamond fillet was seen to have the lowest values of peak-to-peak amplitude, whereas the parabolic fillet had the greatest peak-to-peak amplitude.

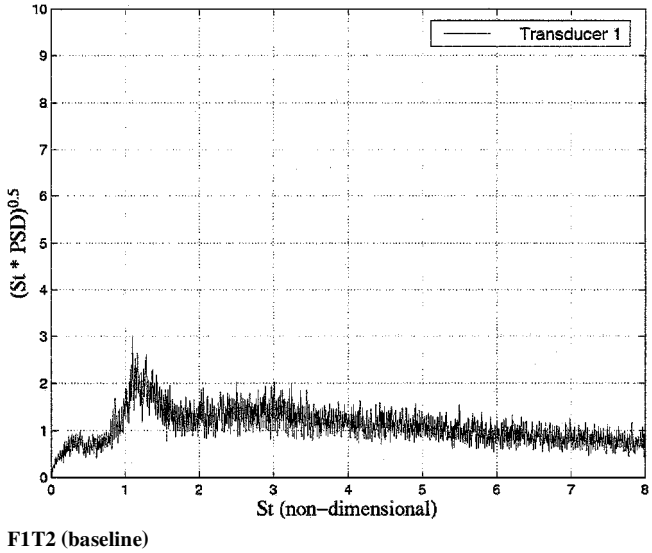

F1T2 (baseline)

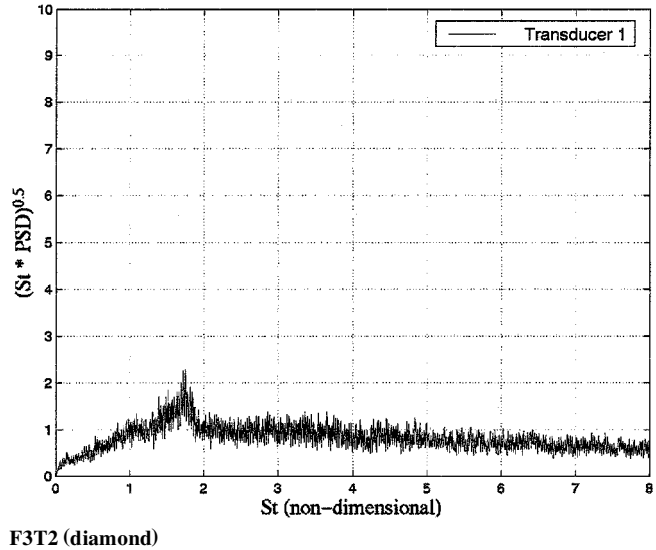

F3T2 (diamond)

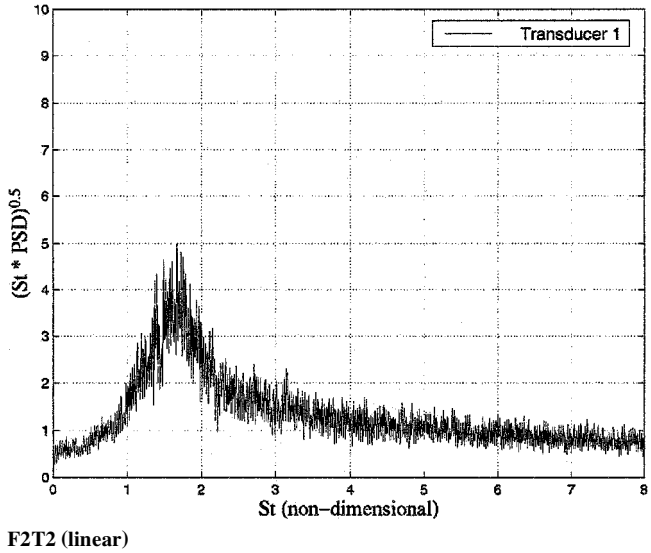

F2T2 (linear)

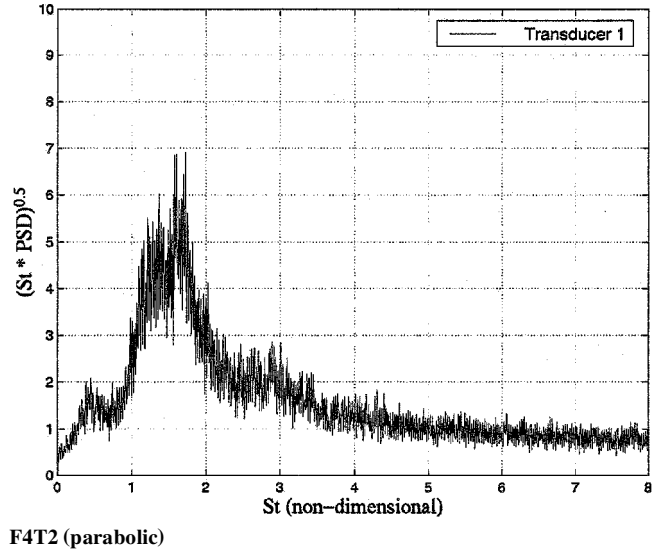

F4T2 (parabolic)

Fig. 14 $(Sr \times \mathrm{PSD})^{0.5}$ vs frequency; transducer 1, $\alpha = 32$ deg.

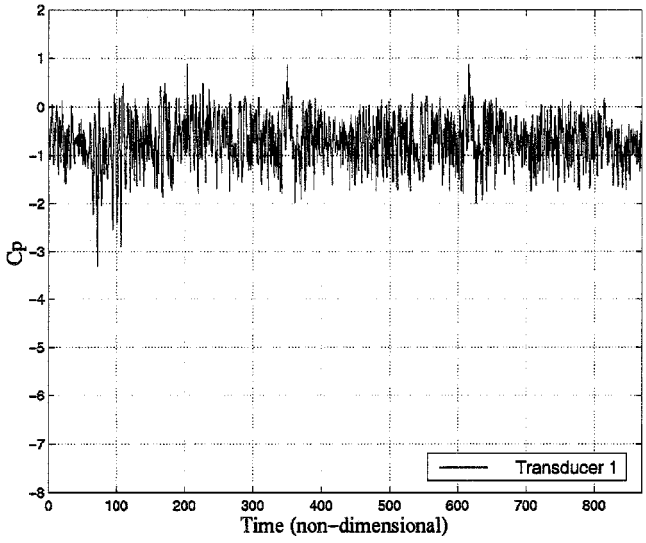

F1T2 (baseline)

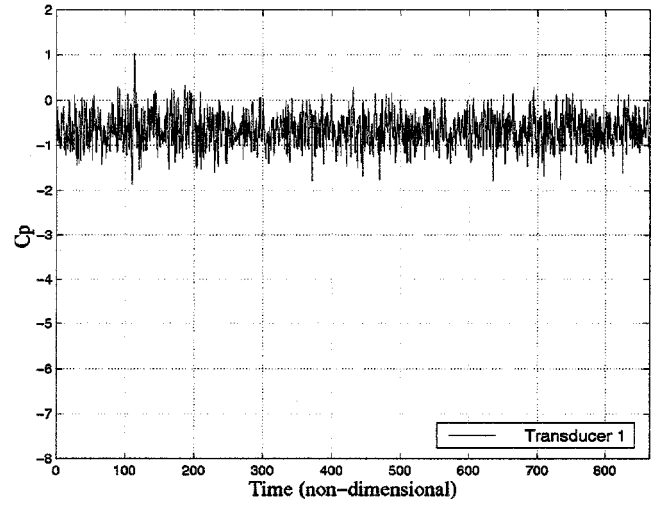

F3T2 (diamond)

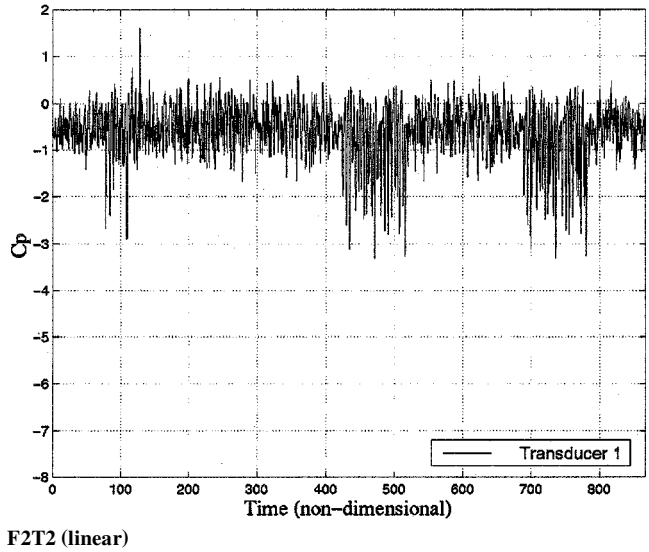

F2T2 (linear)

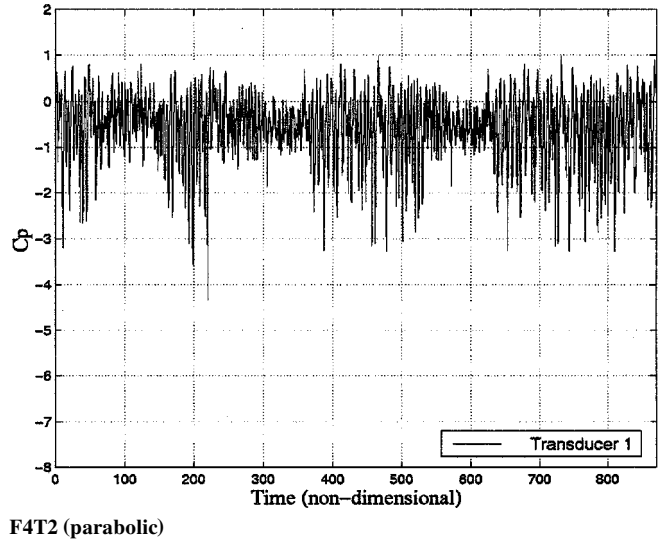

F4T2 (parabolic)

Fig. 15 C_p **vs** τ**, transducer 1,** $\alpha = 32$ **deg.**

Conclusions

A test was conducted to determine the effect of LEX vortex buffet response on a set of pressure-instrumented tails mounted on a 76/40 deg double-delta wing model. Spanwise tail position, angle of attack, and LEX/wing juncture fillet shape were varied parametrically and found to have an effect on the buffet pressure response on the rigid vertical tails. Measured pressure time histories and PSDs were evaluated for each transducer for 35 configurations. Buffet pressure response was seen to vary with angle of attack. Buffet frequency depended on transducer location on the vertical tail as well as fillet shape, spanwise tail location, and angle of attack. The diamond fillet caused the buffet pressure amplitude to decrease and the characteristic frequency to increase. Such a frequency shift may further alleviate tail buffet by moving the characteristic frequency away from the vertical tail natural frequency. Therefore, the diamond fillet shape is a strong candidate for use to alleviate tail buffet.

Acknowledgments

The research was supported by the Office of Naval Research. William King was the Program Manager. Computer resources provided by Department of Defense High Performance Computer facilities located at U.S. Army Research Laboratory, Aberdeen, Maryland.

References

[1]Washburn, A. E., Jenkins, L. N., and Ferman, M. A., "Experimental Investigation of Vortex–Fin Interaction," AIAA Paper 93-0050, Jan. 1993.

[2]"HTP-5 Workshop on Vortical Flow Breakdown and Structural Interactions," NASA Langley Research Center, Hampton, VA, Aug. 1991.

[3]Kandil, O. A., Sheta, E. F., and Massey, S. J., "Twin Tail/Delta Wing Configuration Buffet due to Unsteady Vortex Breakdown Flow," *Proceedings of the 14th AIAA Applied Aerodynamics Conference*, AIAA, Reston, VA, 1996, pp. 1136–1150.

[4]Findlay, D., "Numerical Analysis of Vertical Tail Buffet," AIAA Paper 97-0621, Jan. 1997.

[5]Zimmerman, N. H., and Ferman, M. A., "Prediction of Tail Buffet Loads for Design Application Volume I," U.S. Naval Air Development Center, Rept. NADC-88043-60, Warminster, PA, July 1987.

[6]Kern, S. B., "Vortex Flow Control Using Fillets on a Double-Delta Wing," *Journal of Aircraft*, Vol. 30, No. 6, 1993, pp. 818–825.

[7]Kern, S. B., "Investigation of Vortex Flow Control Using Fillets at the Strake/Wing Junction of a Double-Delta Wing," M.S. Thesis, Dept. of Aerospace Engineering, Pennsylvania State Univ., University Park, PA, May 1992.

[8]Gonzalez, H. G., Erickson, G. E., McLachlan, B. G., and Bell, J. H., "Effects of Various Fillet Shapes on a 76/40 Double Delta Wing from Mach

0.18 to 0.7," *Proceedings of the NATO Applied Vehicle Technology Panel (AVT) Symposium on Advanced Flow Management Part A—Vortex Flows and High Angle of Attack*, MP-69-P-48, May 2001.

[9]Hebbar, S. K., Platzer, M. F., and Alkhozam, A. M., "Investigation into the Effects of Juncture Fillets on the Vortical Flow over a Cropped Double-Delta Wing," AIAA Paper 94-0626, Jan. 1994.

[10]Hebbar, S. K., Platzer, M. F., and Alkhozam, A. M., "Experimental Investigation of Vortex Flow Control Using Juncture Fillets on a Cropped Double-Delta Wing," AIAA Paper 95-0649, Jan. 1995.

[11]Schultz, M. P., and Flack, K. A., "Experimental Investigation of Lift Modification on Double-Delta Wings Using Fillets for 3-D and Flat Plate Models," AIAA Paper 2001-2408, Aug. 2001.

[12]Bendat, J. S., and Piersol, A. G., *Engineering Applications of Correlation and Spectral Analysis*, Wiley, New York, 1980, p. 54.

[13]Welch, P. D., "The Use of Fast Fourier Transform for the Estimation of Power Spectra: A Method Based on Time Averaging Over Short, Modified Periodograms," *IEEE Transactions on Audio and Electroacoustics*, Vol. AU-15, June 1967.

[14]Mabey, D. G., "Some Aspects of Aircraft Dynamic Loads Due to Flow Separation," AGARD-R-750, 1988.

[15]Rae, W. H., and Pope, A., *Low-Speed Wind Tunnel Testing*, 2nd ed., Wiley, New York, 1984, pp. 479–481.